ISSN: 2688-8645

Multi-objective Optimization of Flat Plate in BV500 Seismic Vibrator based on Topology Optimization and Response Surface Method

Xiaozhen Luo, Zhiqiang Huang, Gang Li

School of Mechatronic Engineering, Southwest Petroleum University, Chengdu, Sichuan, 610500, China

Abstract

Aiming at the problems of low vibration energy down-transmission rate and poor quality of excitation signals of the BV500 seismic vibrator in cement road operation, this paper proposes a new multi-objective optimization strategy based on the synergy of topology optimization (TO) and response surface optimization (RSM), which aims to reduce the mass of the flat plate and improve the stiffness of the flat plate. Topology Optimization allocates the plate material to innovatively design an octagonal I-beam plate, while Response Surface Methodology further corrects and optimizes the structural parameters of the plate. The optimization results show that the mass of the new octagonal I-beam flat plate is reduced by 32.08% and the stiffness is increased by 57.13% compared with the traditional aluminum alloy flat plate. The field test verifies that the new flat plate, under the working conditions of 3-96Hz sweep and single frequency (20/50/80Hz), the maximum enhancement of near-field vibration velocity RMS (V_{RMS}) is 42.99% (80Hz), and the enhancement of far-field signal is up to 86.30% (50Hz), which significantly improves the efficiency of medium and high-frequency energy transfer. The results show that the new octagonal I-beam flat plate has better excitation performance.

Keywords

BV500 Seismic Vibrator; Topology Optimization and Response Surface Method; Multi-objective Optimization.

1. Introduction

With the transition of global oil and gas exploration to deep/ultra-deep and unconventional oil and gas, the center of gravity of shale gas development in China has been focused on the Sichuan and Chongqing regions. The shale gas reserves in this region account for more than 40% of the national total [1][2][3], but its complex topography (mountains, plateaus, and hills account for about 90% of the total) has resulted in exploration operations being limited to concrete roads in the countryside, and the BV500 seismic vibrator, as the main exploration equipment in this region, faces significant energy attenuation (flat plate structural dissipation accounts for about 90% of the total) and signal aberration (signal aberration increases about 30%) [4], which severely limits the exploration accuracy. Therefore, based on the optimization of the flat plate structure to enhance the excitation performance on the concrete pavement, it becomes a key breakthrough to improve the excitation efficiency of the seismic vibrator.

In the field of seismic source plate optimization, the existing research mainly focuses on material and structural innovations: Wei revealed the dominant role of plate stiffness on the energy transfer efficiency through the establishment of a plate-geodesic coupling finite element model [5]and verified the mass-bottom-area coupling effect [6]; IVI adopted an elliptical plate with an iron pot-like skeleton design, which resulted in the improvement of stiffness and the increase of the energy downward rate [7]; INOVA develops carbon fiber composite flat panels,

ISSN: 2688-8645

resulting in an increase in flat panel stiffness and a decrease in harmonic distortion [8][9]; Hao Lei achieves mass reduction and decoupling rate decrease by airfoil augmentation and weight reduction slot design [10]; Ding Ya-Ping [11] proposes a new type of vibrator structure, and the difficulty lies in finding the balance between mass and stiffness.Wei et al found that the main way to improve the energy transfer rate is mainly implemented by reducing the energy dissipation of the plate as well as the internal energy of the system [12], which is mainly implemented by reducing the mass of the plate and increasing the stiffness of the plate. The above studies show that the synergy of stiffness enhancement and lightweighting through structural optimization is an effective path to break through the bottleneck of the existing technology.

Topology optimization, as an important tool for structural design, has shown remarkable results in the field of mechanical engineering: Zhang Qingyi [13] and others for the double-pendulum angular head shell, with stress ≤ 10MPa and first-order frequency ≥ 80Hz as constraints, to achieve 7.4% lightweighting and dynamic characteristics optimization; Gao Juan and others [14] constraints on the dynamic performance and flexible deformation of the box body, the box body of the optimization of the topological structure of the study, after the optimization, the weight of the box was reduced by 8%, thus achieving the lightweight goal of the design. Jianfeng Zhu [15] in order to improve the structure of automotive gearbox, through SIMP method topology optimization, based on the manufacturing process, the optimized structure enhances the stiffness of the automotive gearbox, and the mass is reduced by 10%. Yao-Bo Wang [16] used the topology optimization method to study the optimization of angular head gimbal, and finally the mass of the gimbal main structure was relatively reduced by 15%.Yuan [17] optimized a marine gearbox based on the SIMP method, and maintained the static factor of safety ≥ 2.5 while the mass was reduced by 15%. Chenglong Wang et al. [18] Topology optimization is used to assign the material distribution of the valve edge and provide parameters for response surface optimization, while the response surface method optimization further corrects and optimizes the structural parameters of the valve edge, and the results show that the optimized valve has good structural safety and sealing performance. Tan Zhou et al. [19] optimized the mass and stiffness of the spindle of a five-axis grinding machine based on the response surface method, which ultimately led to a 27.35% reduction in the maximum deformation of the spindle and a 3.81% reduction in mass.Tian Aly et al. [20] used the structural deformation and equivalent stresses of steel polyurethane sandwich panels (SPS) as the optimization objective, and the structural dimensions and mass as the constraints, to develop a response surface model to optimize the design of SPS hatch covers. Zheng Lan [21] investigated the effects of different lengths, widths and heights of bionic fins on the thermal performance of plate-fin heat sinks and carried out a multi-objective optimization to obtain the optimal structural parameters of the bionic fins. However, there is still a gap in the technique in the optimization of seismic flat plates.

In this study, a two-stage multi-objective optimization strategy is proposed by combining topology optimization and response surface method optimization. The optimization scheme aims to optimize the flat plate material distribution and obtain the best combination of structural parameters. In the first stage, topology optimization is performed to achieve the optimal layout of flat plate materials with the objective of structural stiffness. Since the optimized model is not convenient for direct manufacturing, it is improved. In the second stage, the central combination design method of response surface method is used to establish multiple response surface models of structural parameters with mass and maximum deformation. The optimal combination scheme of structural parameters is obtained.

ISSN: 2688-8645

2. Vibrator-Concrete Road Finite Element Modeling

2.1. BV500 Seismic Vibrator

Compared with other seismic vibrator vehicles, BV500 has a smaller volume and tonnage, which is convenient to drive on the rural cement roads in Sichuan and Chongqing [18] (Figure 1), and usually generates seismic waves by the vertical vibration of the vibrator located in the middle of the body. The vibrator is mainly composed of gusset plate, guide post, piston rod, reaction mass, hydraulic pressure system, gravity compensation airbag, flat plate and other components, as shown in Fig. 2. As one of the main components of the controlled vibration source, the flat plate is always in contact with the earth coupling during the working process, and its structure will directly affect the excitation effect.BV500 seismic vibrator adopts aluminum alloy integral flat plate, which has the problem of low energy downward transmission rate, etc. In this study, the I-beam flat plate is used, which has the problem of low energy downward transmission rate. This study is the I-beam flat plate, the material is 16Mn, using multiple 16 I-beam welding molding. Compared with the aluminum alloy flat plate, the quality is lighter and the stiffness is greater, and its structure is shown in Figure 3.

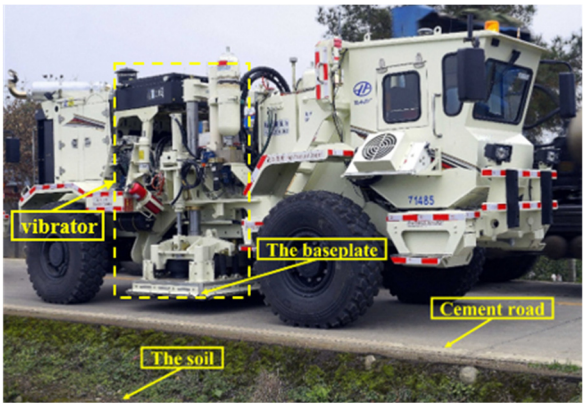

Fig 1. BV500 vibroseis on cement road

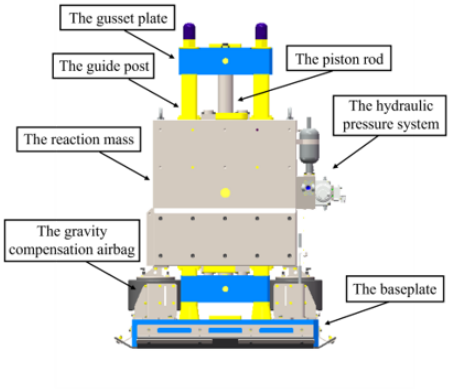

Fig 2. Vibrator structure

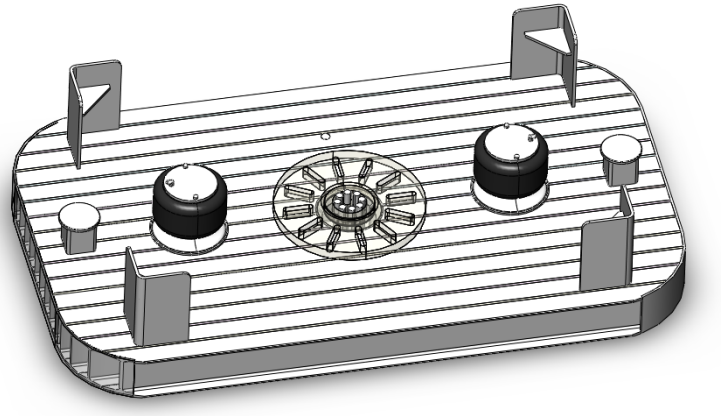

Fig 3. I-steel flat plate structure

2.2. Model of Vibrator-Concrete Roadway Coupling

Considering that the vibrator consists of many structures that have little impact on the simulation, the vibrator structure was simplified in order to reduce the simulation run time (Figure 4). The vibrator is simplified into a flat plate and a upper structure. Among them, the upper structure consists of The gusset plate, 4 guide post, the piston rod in the middle and the baseplate, and the material is 45 steel; simplify the vibration isolation airbag on the flat plate to 8 supports, and at the same time, delete the 4 chamfers and other structures on the flat plate,

ISSN: 2688-8645

so as to get the simplified I-beam flat plate (Table 1 for the specific dimensional information) consists of the upper and lower two flange plates (thickness of 10mm) and 14 pieces of web plates (thickness of 6mm). Most of the rural cement roads in Sichuan and Chongqing are made of cement pavement on the upper layer and soil on the lower layer. Through many field measurements, it is found that the thickness of most of the rural cement roads in Sichuan and Chongqing is between 0.1-0.13m, so the thickness of the cement road is taken as 0.1m; at the same time, it can be seen from the relevant literature that most of the top layer of the soil in Sichuan and Chongqing is hard soil. Thus, in order to characterize the actual geodetic situation as much as possible, a two-layer geodetic model of cement road and hard soil was established (see Table 1 for specific dimensional information). The coupled vibrator-earth model is shown in Fig. 4.

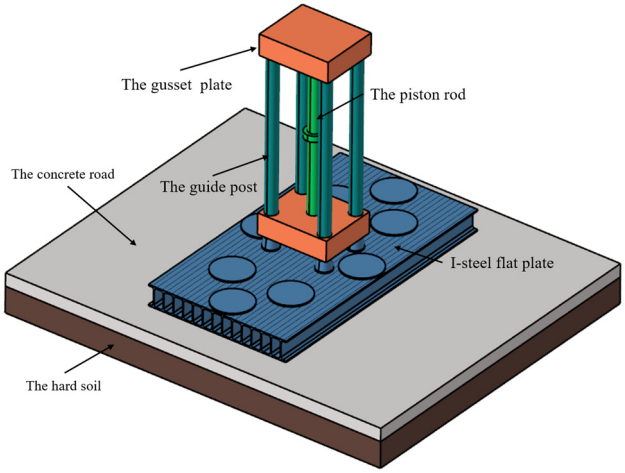

Fig 4. Vibrator-earth coupling model

Table 1. Earth and flat plate dimensions

	Length (m)	Width (m)	Thickness (m)
I-steel flat plate	2	1.1	0.16
Cement road	3	2.5	0.1
Hard soil	3	2.5	0.2

2.3. Material Setting and Grid Painting

When the BV500 seismic vibrator operates on the concrete road, the deformation of the vibrator flat plate, the road and the earth can be considered to be in the elastic deformation stage. Based on this, a linear elastic model is chosen for the material's intrinsic model, and the specific parameters are shown in Table 2.

Table 2. Material parameter characteristics

Parts	Materials	Density(kg/m^3)	Elastic modulus(Mpa)	Poisson ratio
I- steel flat plate	16Mn	7850	212000	0.31
Above-flat plate structure	45steel	7890	209000	0.27
Cement road	Concrete	2600	30000	0.26
Earth	Hard soil	1800	200	0.32

The grid size of cement road and hard soil is 100mm (meet the wavelength criterion ≤ λ_min/20, when f=50Hz, λ_min=10m); due to the web thickness of No.16 I-beam is 6mm, in order to

ISSN: 2688-8645

analyze it more accurately, the minimum grid size is set to be 3mm; the hexahedral mesh is used for piston rods and guide columns, and the mesh size is 10mm; the mesh size of the rest of the parts is 20mm. The meshing results are shown in Fig. 5.

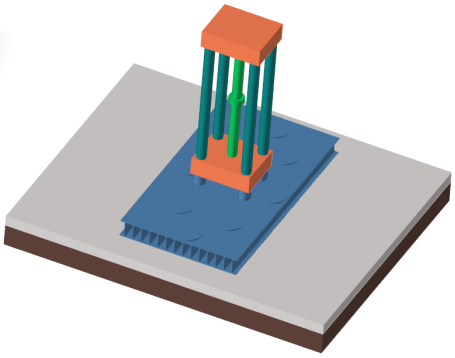

Fig 5. Grid division

2.4. Loads and Boundary Conditions

The loads to which the vibrator is subjected during operation can be simplified into static loads and dynamic loads. The static load includes the weight of the reaction mass and the pressure of the controlled vibration source vehicle. The pressure of the reaction mass is simplified to act directly on the two dark blue baseplate, while the gravity of the controlled vibration source vehicle is simplified to act on the six light blue baseplate (shown in Fig. 6), and the two pressurized weights are combined into one as shown in Fig. 6, with a peak load value of 45 KN, and the time of application is from 0s to 1s to ensure that the flat plate adheres closely to the ground during vibrator excitation. Make sure that the vibratory excitation process of the flat plate and the earth are close together. Dynamic load is a periodic sinusoidal hydraulic pressure pumped by the hydraulic pump, this simulation will be the output of the hydraulic oil high-pressure signal converted into force signal load (shown in Figure 7), the peak value of the output force of 154kN, in order to facilitate the simulation of the study, the signal frequency is set to 50Hz (single frequency), in order to obtain a more complete simulation results, the setting of 25 excitation cycle (0.5s to 1s), the role of the piston rod cam at the upper and lower end of the platform. The signal frequency was set to 50 Hz (single frequency), and to obtain more complete simulation results, the setting of 25 excitation cycles (0.5s to 1s), Acting on the piston rod boss.

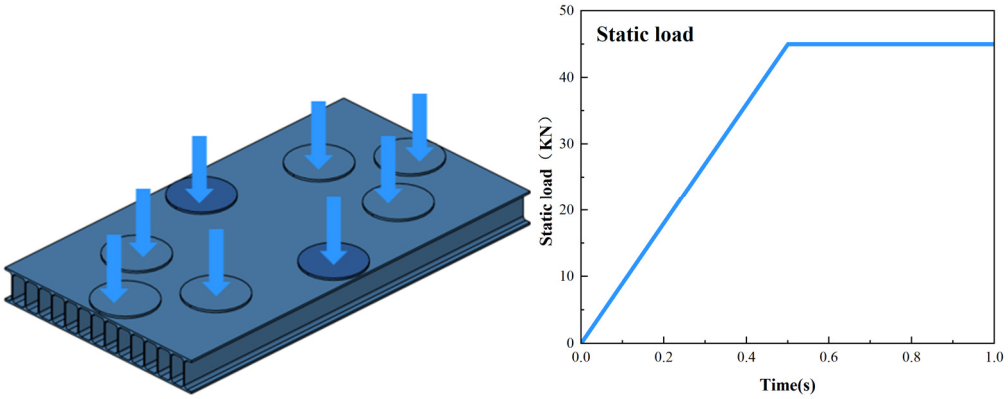

Fig 6. Static load loading position and curve

From the above, it can be seen that the presence of static load makes the relative displacement between the earth and the vibrator during the operation of the seismic vibrator very small, so the completely fixed constraints are imposed on the bottom surface and four sides of the earth. At the same time, in order to prevent the phenomenon of rebound of seismic waves arriving at

ISSN: 2688-8645

the boundary in the simulation, the bottom surface and four sides of the earth model are imposed with the non-reflective boundary conditions [5][16 young master].

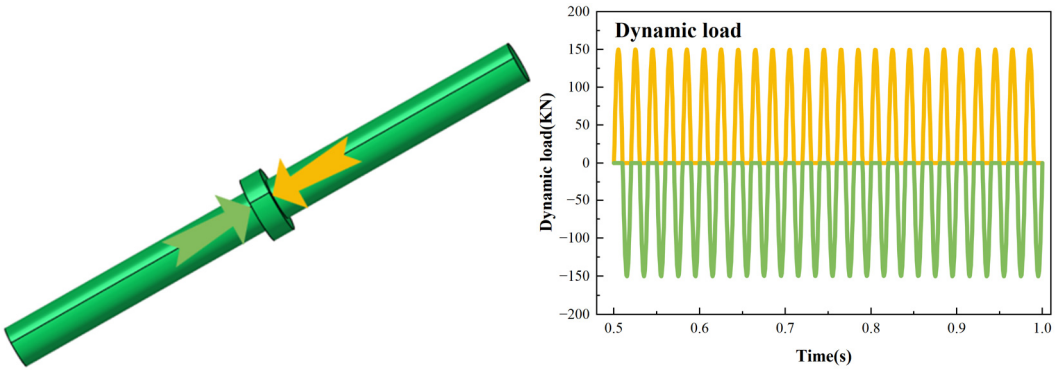

Fig 7. Dynamic load loading curve and position

2.5. Validation of Finite Element Model

To ensure the accuracy of the finite element analysis results, the established vibrator-cement road finite element model should be validated first. The flat plate acceleration of the BV500 seismic vibrator during excitation on the cement road was extracted and compared with the flat plate acceleration obtained from the simulation model (e.g., Table 3). The results show that (1) the difference between the amplitude and the average value of the simulated acceleration and the test acceleration is small, and the relative errors are 7.73 % and 5.13 %, which can prove the accuracy of the established finite element model; (2) due to the systematic error, the test acceleration is presented as an aberrant sinusoidal waveform, and the periods of the two are more in line with each other, which can prove the feasibility of the established road excitation model.

Table 3. flat plate acceleration amplitude and average value comparison

Groups	Test group	Simulation group	Relative error
flat plate acceleration amplitude(m/s^2)	71.16	76.66	7.73 %
Average flat plate acceleration(m/s^2)	-0.039	-0.041	5.13 %

3. Design of Octagonal I-steel Flat Plate Based on Topology Optimization

3.1. Topology Optimization Mathematical Model of SIMP Method

The variable density method is widely regarded as one of the main approaches to deal with continuum topology optimization [23][24][25], using the relative density of the material in the finite element cell as a variable for the optimal design.Solid Isotropic Material with Penalization (SIMP) is one of the frequently used mathematical models in topology optimization with the following expression:

$$E_i = \rho(x_i)^p E_0 \tag{1}$$

Where E_i - elastic model for the calculation of the stiffness matrix; ρ(xi) - relative density of the unit material;E_0 - the elastic modulus of the material itself;P - penalty factor (generally takes the value of 3).

The optimization objective is determined to be the maximum stiffness of the flat plate, the design variable is the density of the material in each cell in the flat plate, and the constraint is that the volume fraction of the constrained design domain of the flat plate is less than 30%.

ISSN: 2688-8645

Combined with the finite element numerical method, the structure is discretized into n units and the density function is discretized into an N-dimensional vector, which is assumed to be:

$$X = (x_1, x_2, \cdots, x_n) \tag{2}$$

Where x_i - the pseudo-density value of cell i, expressing the presence or absence of material in each cell, $x_i = 0$ for no material and $x_i = 1$ for material.

$$\begin{cases} find\ X = (x_1, x_2, \cdots, x_n) \\ \min\ C(X) \\ s.t.\ v = \dfrac{\sum_{i=1}^{n} x_i v_i}{V_0} \le f \\ KU = F \\ 0 < x_{\min} < x_i \le 1 \end{cases} \tag{3}$$

Where v_i - the ith unit volume; V_0 - volume of flat plate structure; f - upper limit of volume fraction ratio; x_{min} - very small positive number to avoid stiffness matrix singularity in finite element calculations; KU = F - finite element equilibrium equation; K - overall stiffness matrix of the structure; U - overall displacement vector of the structure; F - overall load vector of the structure.

The optimization objective in the optimization of the flat plate topology of the controlled source vibrator is to maximize the stiffness of the flat plate structure, and this optimization problem can be converted into a flat plate structure flexibility minimization problem, i.e., the objective function in Eq. is set as:

$$C(X) = F^{\mathrm{T}}U = U^{\mathrm{T}}KU = \sum_{i=1}^{n} \rho(x_i)^p u_i^T k_0 u_i \tag{4}$$

Where u_i - displacement vector of the ith cell; k_0 - unit stiffness matrix of the flat plate structure.

3.2. Flat Plate Topology Optimization Results and Validation

The topology optimization cloud obtained by the SIMP method (Fig. 8a) shows that the material removed by the topology optimization is mainly in the four corner regions of the non-primary load-bearing area. The optimized model (Fig. 8b) removes about 32% of the volume of material, achieving a reduction in mass and an increase in stiffness. In order to verify the accuracy of the topology optimization of the flat plate, dynamic simulation analysis was performed. The transient dynamics simulation showed that the flat plate buckled at four corners under 50 Hz excitation with a maximum displacement of 1.051 mm (Fig. 9), which verified the accuracy of the topology optimization. In order to address the difficulty of direct manufacturing of the topology optimization model, the four corners of the flat plate were removed, and an engineering feasible octagonal I-beam flat plate was innovatively designed (Fig. 10).

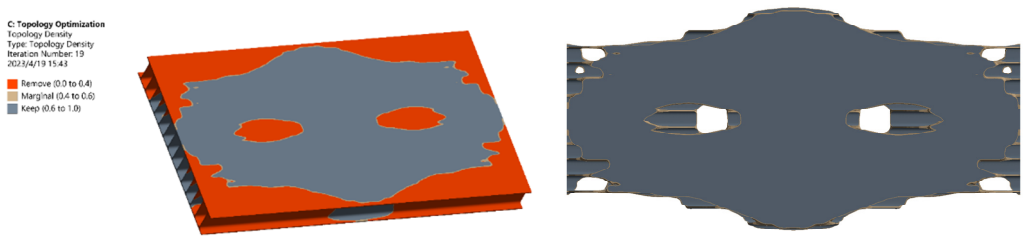

(a) Topology optimization analysis cloud (b) After removing the material

Fig 8. Flat flat plate topology optimization results

ISSN: 2688-8645

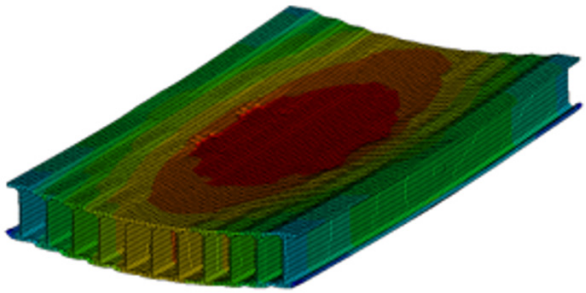

Fig 9. Flat plate dynamics simulation

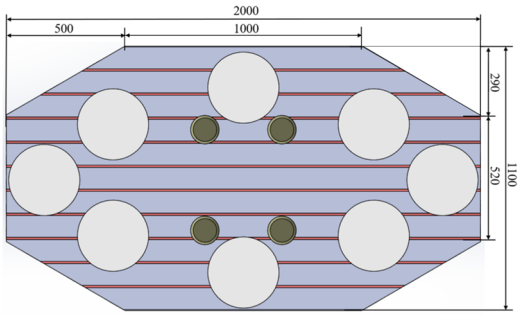

Fig 10. Octagonal I-steel flat plate

4. Optimized Design of Octagonal I-Beam Flat Plate based on Response Surface Optimization

4.1. Establishment of Optimization Objectives and Design Variables

The basic contour dimensions of the octagonal I-beam flat plate are obtained through the topology optimization design, and then the mass and stiffness of the octagonal I-beam flat plate are taken as the optimization objectives (due to the limitation of the software, the maximum deformation is used to replace the stiffness), and the optimization design of the dimensions of the web and the flange plate is carried out. Since part of the intermediate web is mainly subjected to periodic hydraulic pressure, the web is divided into intermediate and lateral webs, from which four design variables are defined as (shown in Fig. 11): the thickness of the top flange plate of L1, the thickness of the bottom flange plate of L2, the thickness of the intermediate web plate of L3, and the thickness of the lateral web plate of L4. Based on the original dimensions of the octagonal I-beam flat plate, a larger range is used for optimization in this study, and the range of values of L1, L2, L3 and L4 are obtained as shown in Table 4. Since the response surface method needs to take into account the different degree of influence of each parameter on the prediction results in the modeling, 25 groups of experimental design points were constructed in this study by using the center-response composite design of experiments (CCD) method[26][27].

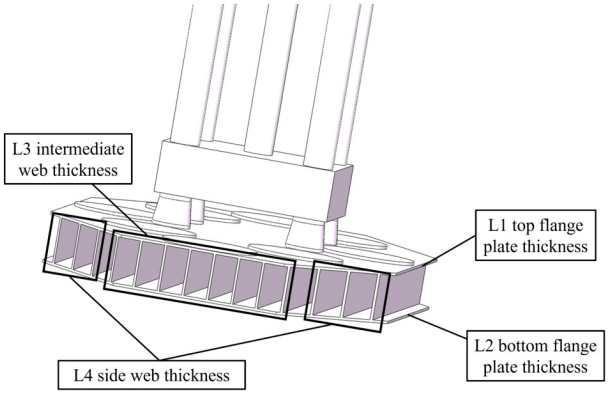

Figure 11. 4 design variables

Table 4. Range of design variables

Size	Initial value(mm)	Variation range(mm)
L1	9.9	2—20
L2	9.9	2—20
L3	6	2—20
L4	6	2—20

ISSN: 2688-8645

4.2. Response Surface Modeling based on Kriging Function Method

ANSYS Workbench provides five methods to build response surface, Kriging model is one of them, and Kriging has the advantages of high fitting of test points and solving highly nonlinear problems compared with other methods[28], so this study applies the Kriging function method for the establishment of response surface model.

Using the response values corresponding to the test points obtained from the central composite experimental design, the samples are input into the response surface, and the response surface model is constructed through the Kriging model, and the mass response surface model is obtained as shown in Fig. 12, and the total deformation response surface model is shown in Fig. 13. The results of the study show that the effects of changes in each design variable on mass and total deformation are significantly different, and there are complex interactions between the parameters.

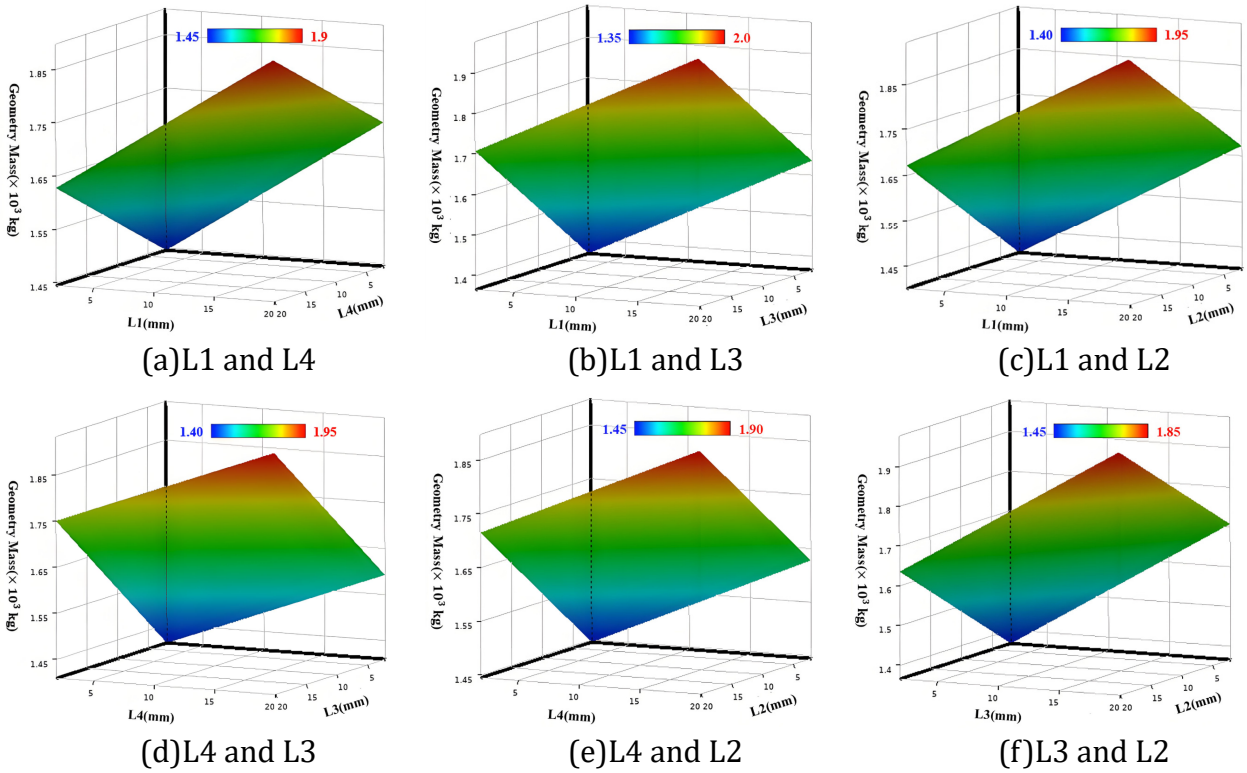

(a)L1 and L4 (b)L1 and L3 (c)L1 and L2

(d)L4 and L3 (e)L4 and L2 (f)L3 and L2

Fig 12. Quality response surface model

In order to more accurately predict the effects of different parameter combinations[29], sensitivity analysis of L1, L2, L3 and L4 was carried out (the results are shown in Fig. 14), and it can be seen from the figure that, L1, L2, L3 and L4 positively affect the quality of the octagonal I-beam flat slabs but the difference in the effects of these four is not large, of which L3 (the thickness of intermediate webs) is the most significant effect; in addition, the effects of L1, L3 and L4 on the deformation of octagonal I-beam flat plate after being loaded into an inverse proportion, L2 on the deformation of octagonal I-beam flat plate after being planted into a positive proportion, of which the influence of L3 (the thickness of the middle web) is the most significant, and is much larger than the other three parameters, which highlights the key role of the intermediate web in the resistance to deformation. In summary, L3 has the greatest influence on the mass of the flat plate and the total deformation after loading than the other three design variables.

ISSN: 2688-8645

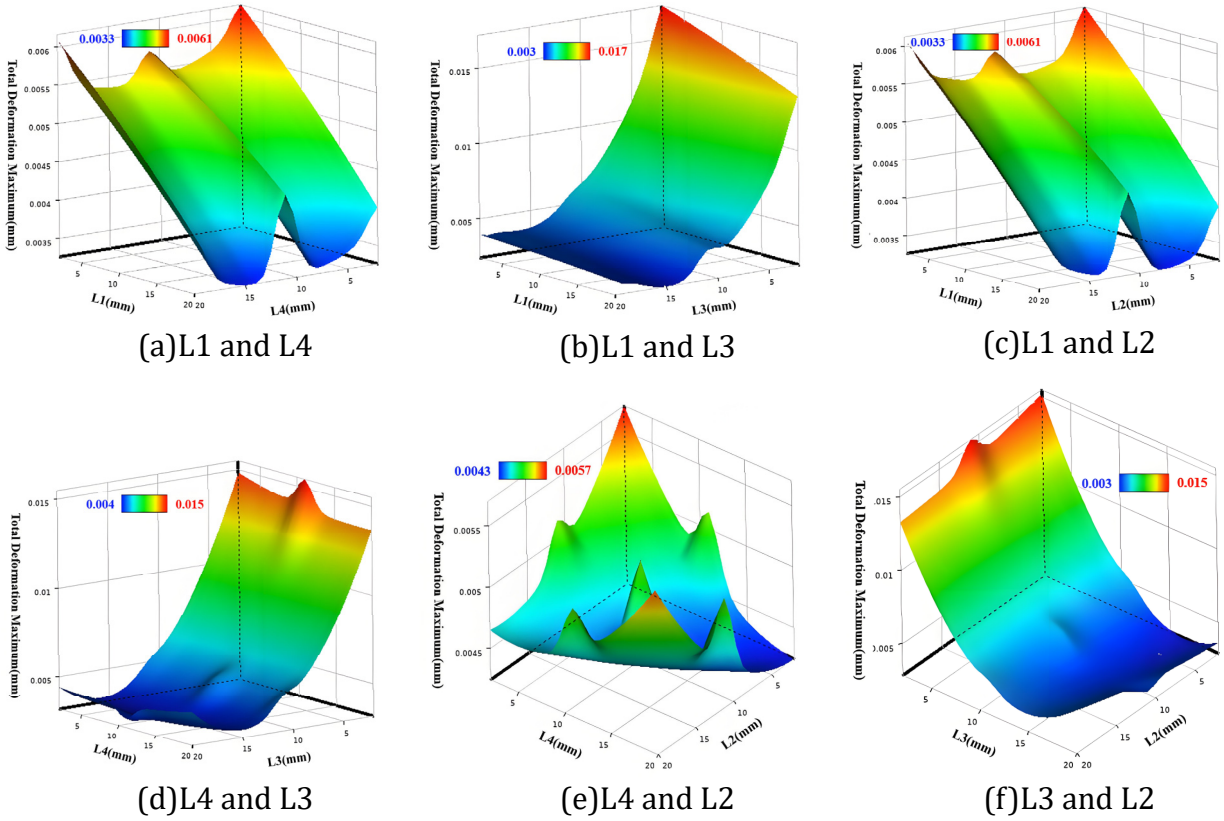

(a)L1 and L4 (b)L1 and L3 (c)L1 and L2

(d)L4 and L3 (e)L4 and L2 (f)L3 and L2

Fig 13. Total deformation response surface model

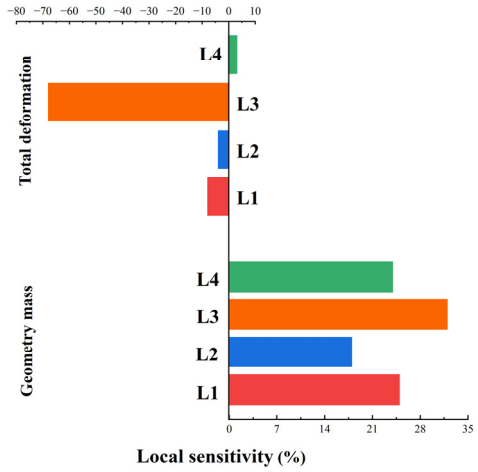

Fig 14. Sensitivity histogram

4.3. Validation of Response Surface Modeling

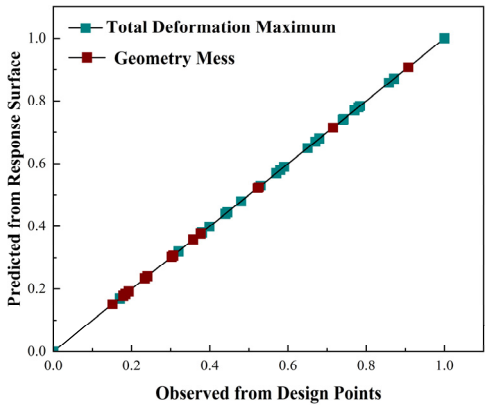

Figure 15. Predicted versus Observed Chart scatterplot

ISSN: 2688-8645

The Predicted versus Observed Chart scatter plot of the two responses is shown in Figure 15. It can be found that the scatter points are basically located in the vicinity of the 45-degree line, and the prediction results are better[30], indicating that the real values of the response variables obtained from the sample design points coincide with the response variables obtained from the response surface model, which indicates that the response surface model constructed based on Kriging has high accuracy and can be used for subsequent analysis.

5. Multi-objective Optimization of Octagonal I-beam Flat Plate

5.1. Optimization Design Principle

MOGA is an efficient non-dominated sorting method, which is especially suitable for finding the global optimal design and can be applied to the response surface optimization system at the same time[28] . For the octagonal I-beam flat plate, it should be ensured that the deformation of the flat plate after being loaded is reduced on the basis of its minimum mass, i.e., the multi-objective optimization design of the octagonal I-beam flat plate is carried out on the premise of ensuring the maximum stiffness under the premise of its smaller mass.

The mass and deformation of the octagonal I-beam flat plate are selected as the objective function, and the expression of the objective function is as follow:

$$G(X)=\{\min(M),\min(D)\} \tag{5}$$

Where G (X) - objective function;M - mass of octagonal I-beam flat plate (kg);D - deformation of octagonal I-beam plate after loaded (mm).

From this, we can get the mathematical model for the optimization of octagonal I-beam flat plate as follows:

$$\begin{cases} Find\ L=[L_1,L_2,L_3,L_4] \\ 2\text{mm}\le L_1\le 20\text{mm} \\ 2\text{mm}\le L_2\le 20\text{mm} \\ 2\text{mm}\le L_3\le 20\text{mm} \\ 2\text{mm}\le L_4\le 20\text{mm} \\ s.t.\ G(X)=\{\min(M),\min(D)\} \end{cases} \tag{6}$$

5.2. Analysis of Optimization Results

Based on the optimization results, the Pareto front points are generated as shown in Fig. 16, and the three groups of best optimization schemes are selected from the Pareto front sample points as shown in Table 5. Comparing and analyzing the three optimization schemes, it is found that the mass size of the third optimization scheme is not much different compared with the first and second optimization schemes, but the deformation of the flat plate is smaller compared with the other two groups, so the third optimization scheme is selected as the final value of the multi-objective optimization for comprehensive consideration. Comparing the results before and after the multi-objective optimization (Table 6), the total mass of the octagonal I-beam flat plate is reduced from 1493kg to 1445.1kg, which is 32.08%; the deformation of the octagonal I-beam flat plate after being loaded is reduced from 9.0992E-03mm to 3.9011E-03mm, which is 57.13%. Therefore, this study shows that the designed octagonal I-beam flat plate has smaller mass and deformation compared with the prototype flat plate, and theoretically has better excitation performance. Based on this multi-objective optimization result, and also combined with the actual model of I-beam, the dimensions are rounded to obtain the optimized model as shown in Fig. 17.

ISSN: 2688-8645

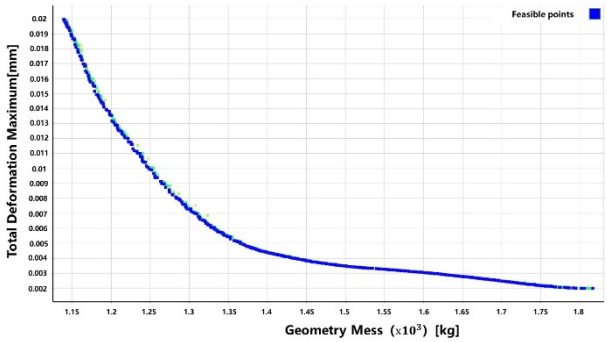

Fig 16. Pareto front points

Table 5. Three best optimization schemes

optimization scheme	L1(mm)	L2(mm)	L3(mm)	L4(mm)	quality (kg)	deflection (mm)
1	2.001	2.0015	15.003	2.002	1386.2	4.5808E-03
2	2.047	2.0238	15.232	4.611	1418.1	4.1872E-03
3	2.0395	2.0015	15.366	7.0636	1445.1	3.9011E-03

Table 6. Compared with the original design after multi-objective optimization

Exponential parameter	Original design	After optimization	Rate of change
deflection(mm)	9.0992E-03	3.9011E-03	-57.13%
quality (kg)	2125.2	1445.1	-32.08%

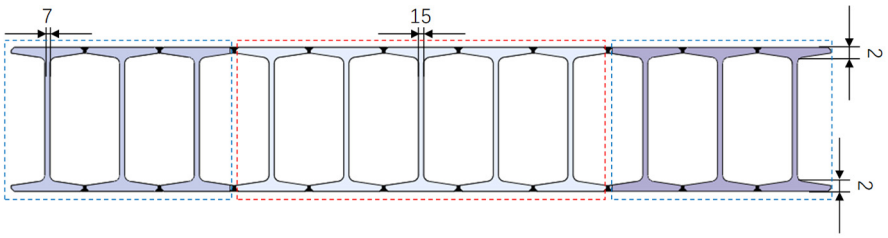

Fig 17. Optimized octagonal I-steel flat plate

The optimized thickness of the middle web is 15mm and the thickness of the side web is 7mm; however, since the thickness of the flange plate and the web of the I-beam is produced according to its model, in order to reduce the mass while taking into account the stiffness of the flat plate, the thickness of the middle web and the thickness of the side web are taken as 7mm.

6. Experimental Study on Excitation Performance of Octagonal I-Beam Flat Plate

6.1. Experiment Equipment and Scheme Design

In order to check the excitation performance of octagonal I-beam flat plate (hereinafter referred to as the new flat plate), the excitation comparison experiment between aluminum alloy flat plate (hereinafter referred to as the prototype flat plate) and the new flat plate was carried out on the concrete surface with BV500 seismic vibrator as the carrier, as shown in Figure 13. In order to comprehensively test the excitation performance of the new flat plate in the low, medium and high frequency bands, this test adopts two loading methods: continuous frequency sweep and single frequency, the continuous frequency sweep ranges from 3 to 96 Hz, and the single frequency excitation selects the representative values of the low, medium and high frequency bands: 20 Hz, 50 Hz and 80 Hz, and the loading time is 12 s.

ISSN: 2688-8645

(a) Prototype flat plate (b)new flat plate

Fig 18. New flat plate excitation test

6.2. Velocity RMS(V_{RSM})

The signals received by the geophones within 20 m from the source vehicle are called near-field signals, and the signals received by the geophones beyond 20 m from the source vehicle are called far-field signals. In order to characterize the excitation performance of the flat plate, the vibration velocity RMS (V_{RMS}) [41] is introduced to represent the magnitude of the vibration energy during the loading process, which can be expressed as:

$$V_{RMS} = \sqrt{\frac{\sum_{i=1}^{N} x^2}{N}} \tag{7}$$

Where V_{RMS} - effective value of vibration velocity;i - the ith time point;N - number of discrete time points;x - vibration velocity at the ith point in time.

6.3. Experimental Results

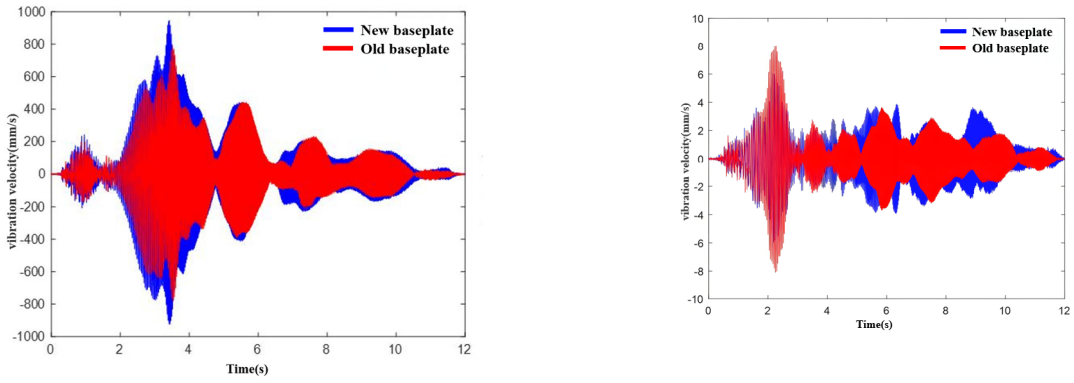

(a)nearfield signal (b)far-field signal

Fig 19. Signals under continuous sweep loading mode

Fig. 19 shows the vibration velocity-time curves for the continuous sweep loading mode from 3 to 96 Hz. The calculated V_{RSM} enhancement rate is shown in Fig. 21. Both in the near-field and far-field, the new flat plate is enhanced compared with the prototype flat plate. In the near-field signal, the new flat plate is improved by 34.18% compared with the prototype flat plate, and in the far-field signal, the new flat plate is improved by 17.39% compared with the prototype flat plate. Therefore, in the frequency sweeping, the new flat plate has greater excitation strength

ISSN: 2688-8645

and better excitation performance, which is more conducive to the exploration effect of BV500 seismic vibrator.

Fig. 20 shows the vibration velocity-time curve of the near-field signal under the single-frequency loading mode. The calculated V_{RMS} enhancement is shown in Fig. 21. In the V_{RMS} of the near-field signal, the increase of the low-frequency 20Hz section is small; the mid-frequency 50Hz section has a larger enhancement of 21.52%; and the high-frequency 80Hz section has a huge enhancement of a staggering 42.99%, which indicates that the excitation effect of the new flat plate is superior to the prototype flat plate to varying degrees, especially in the middle and high frequency bands. It shows that the excitation effect of the new flat plate is better than that of the prototype to different degrees, especially in the middle and high frequency bands. In the V_{RMS} of the far-field signal, the low-frequency 20Hz section has a large improvement, reaching 36.58%; the mid-frequency 50Hz section has a huge improvement, reaching an amazing 86.30%; and the high-frequency 80Hz section has a small increase, which indicates that the excitation effect of the new flat plate is superior to the prototype flat plate to different degrees, especially in the middle and low-frequency bands have larger improvement. In summary, the excitation effect of the new flat plate is better than that of the prototype flat plate both in the near field and far field, and the enhancement in the near field part is mainly concentrated in the middle and high frequency bands, while the enhancement in the far field part is mainly concentrated in the middle and low frequency, which can effectively enhance the exploration effect of BV500 seismic vibrator in the cement road surface.

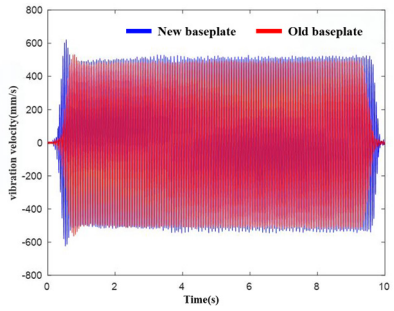

(a)20Hz near-field signal

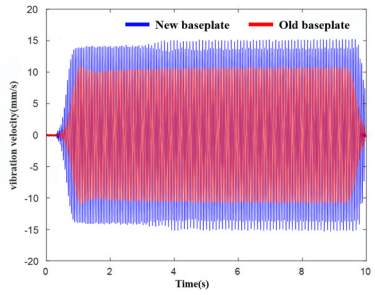

(b)20Hz far-field signal

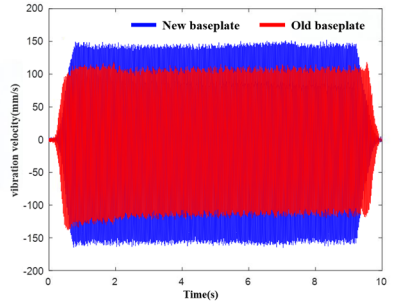

(c)50Hz near-field signal

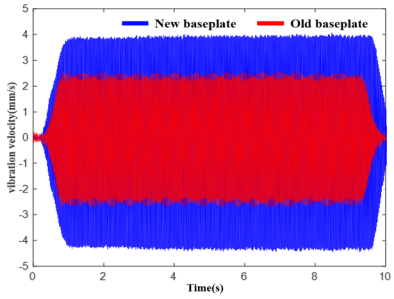

(d)50Hz far-field signal

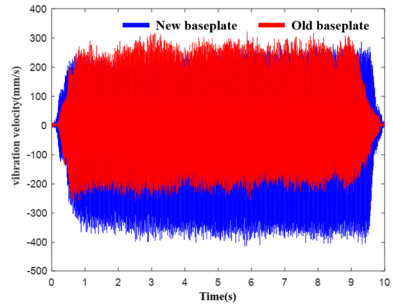

(e) 80Hz near-field signal

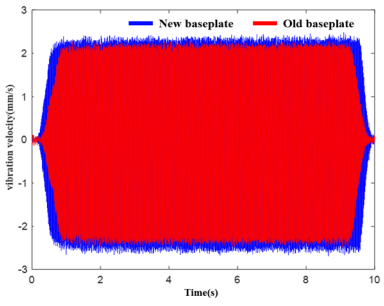

(f)80Hz far-field signal

Fig 20. Signal under single frequency loading mode

ISSN: 2688-8645

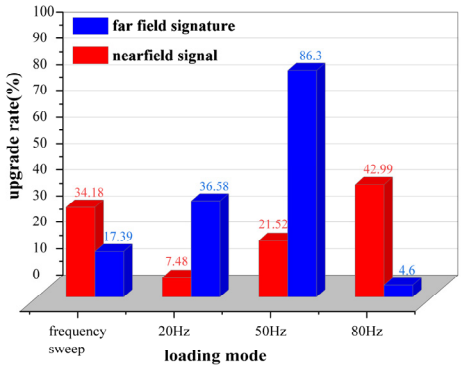

Fig 21. V_{RMS} upgrade rate

7. Conclusion

This study optimized the I-beam flat plate based on topology optimization and response surface optimization, significantly enhancing the excitation performance of the BV500 seismic vibrator on cement roads. A new octagonal I-beam flat plate was designed through SIMP topology optimization and MOGA multi-objective optimization, achieving reduced mass and increased stiffness. Experiments revealed that the new flat plate showed improvements over the prototype flat plate in both the near-field and far-field. The specific conclusions are as follows:

(1) The prototype flat plate was optimized using the SIMP method, removing approximately 32% of the material volume, achieving reduced mass and increased stiffness. Based on engineering practicality, a new octagonal I-beam flat plate was designed.

(2) The flange plate and web plate were optimized through MOGA multi-objective optimization. The deformation of the optimized flat plate was reduced by 57.13%, and the mass was reduced by 32.08%, theoretically resulting in better excitation performance.

(3) The excitation performance of the new flat plate was validated through experiments. Under both frequency sweep and single-frequency loading methods, the new flat plate showed improvements over the prototype flat plate in both the near-field and far-field.

References

[1] Li Jian, She Yuanqi, Gao Yang, et al. Development situation and prospect of natural gas industry in China[J]. Natural Gas Industry, 2020, 40(4): 133.142.

[2] Zou Cai Cai, Guo Jian Lin, Jia Ai Lin, et al. Connotation of scientific development of China's atmospheric fields[J]. Natural Gas Industry, 2020, 40(3):1-12.

[3] Zou Cai Cai, Zhao Qun, Cong Lianzhu, et al. Progress, potential and prospect of shale gas development in China[J]. Natural Gas Industry, 2021, 41(1):1-14.

[4] LI Qin, PU Wei, HUANG Zhi-qiang, XI Yu-xi, LI Gang, WANG Ruo-hao. Analysis of road vibration effect of vibroseis in Sichuan and Chongqing area[J]. Chinese Journal of Engineering Design, 2022,29(6): 766-775.

[5] Wei Z .Modelling and modal analysis of seismic vibrator flat plate[J].Geophysical Prospecting, 2010, 58(1): 19-32.DOI:10.1111/j.1365-2478.2009.00811.x.

[6] Wei Z , Phillips T F .Harmonic distortion reduction on seismic vibrators[J].Leading Edge, 2010, 29 (3): 256-261. DOI:10.1190/1.3353719.

[7] BROOK R A, CREWS G A .Experimental analysis of vibrator flat plate dynamics[J]. Seg Technical Program Expanded Abstracts, 1991, 10(1):1646.

[8] Wei, Zhouhong, PHILIPS T. Seismic vibrator having a composite flat plate: America: US2012/ 0269040A1[P]. 2012-10-25.

[9] FAIR D W. Seismic transducer flat plate and housing assembly[J]. The Journal of the Acoustical Society of America, 1998, 75(6):1930.

[10] HAO Lei. Research and improvement on the effect of controlled vibrating source plate[D]. Chengdu: Southwest Petroleum University, 2014:39-44. (In Chinese).

[11] DING YaPing. Optimization design and effect study of KZ-28 controlled source vibrator plate structure [D]. Chengdu: Southwest Petroleum University, 2015:32-40. (In Chinese).

[12] SALLAS J J. Seismic vibrator control and the downgoing P-wave[J]. Seg Technical Program Expanded Abstracts, 1982, 1(1):732-740.

[13] Zhang Q.Y., Zhang W., Zhang Q.W., et al. Wang JG. Motion simulation and analysis of double pendulum milling head for wood processing based on Solidworks[J]. Woodworking Machine Tools, 2012, (02): 24-27.

[14] MIN Haitao, GAO Juan, MA Tianfei. Strength analysis and optimization design of automotive transmission case[J]. China Mechanical Engineering, 2012, 23(20): 2514-2519.

[15] ZHU Jianfeng, LIN Yi, CHEN Xiaokai et al. Topology optimization design of automotive gearbox housing[J]. Journal of Jilin University (Engineering Edition), 2013, (3): 584-589.

[16] Dong Z. Research on the structural design of direct-drive A/C double pendulum angle milling head for CNC machine tools [D]. Guangdong University of Technology,2015.

[17] Yuan M H, Tong S G, Cai Q. Modal Analysis and Lightweight Design of High-Power Marine Gearbox Based on Topology Optimization[J]. Mechatronics And Intelligent Materials III, PTS 1-3, 2013, 706-708: 1428-1432.

[18] Chenglong Wang, Dongtao Xu, Kaixian Huang, et al. Multi-objective optimization of a triple-eccentric butterfly valve considering structural safety and sealing performance[J]. ISA transactions, 2024, Vol.155: 295-308.

[19] TAN Zhou,LIAO Yinghua, JIANG Jie. Multi-objective optimization of five-axis grinding machine spindle based on second-order response surface method[J]. Machine Design,2022,39(5):122-128.

[20] TIAN Ali,WEI Zhen,ZHANG Haiyan, et al. Multi-objective optimization of SPS hatch cover structure based on response surface method[J]. Ship Mechanics,2021,25(4): 502-508.

[21] Zheng Lan, Si-yu Wu,Chuang-ye Li,et al. Study and optimization of ribbed flat-plate fin heat sink based on placoid scale shape[J]. International Journal of Heat and Fluid Flow, 2024, Vol.110: 109578.

[22] LIU Zhigang, ZHANG Libao, WANG Xianchun, et al. Customized development and application of lightweight BV500 seismic vibrator[C]// Petroleum Physical Exploration Professional Committee of Chinese Petroleum Society, Exploration Geophysics Committee of Chinese Geophysical Society. Proceedings of the 2019 Physical Exploration Technology Symposium of the Chinese Petroleum Society. China Petroleum Oriental Geophysical Company, 2019:1420-1423.

[23] Yue Bo, Xu Yingjie, Xu Ningxin, et al. Topology optimization design of frame mold structure for hot press can forming[J]. Journal of Aeronautics, 2022, 43(3): 541-553.

[24] WANG Yi-wei, LEI Ruiwu, WANG Hui. Structural topology optimization of flying wing layout aircraft[J]. Beijing: Journal of University of Aeronautics and Astronautics, 2023, 49(2): 482-490.

[25] Shen Xiaoxi. Research on topology optimization of tanker structure[D]. Harbin: Harbin Engineering University, 2019:9-18.

[26] WANG Lei, WANG Ming, XING Yipeng. Optimization of machine tool column based on response surface model and genetic algorithm[J]. Journal of Nanjing University of Science and Technology, 2018, 42(4): 453-458.

[27] Lai Daiwei. Optimization of mirror back support structure based on response surface method [D]. China Academy of Engineering Physics, 2019.

[28] Gong Zichao. Design and analysis of a three-dimensional platform for the construction of low and medium-rise steel assembly buildings.

[29] Zhao Chen-Long. Multi-objective optimization of BT50-AVM32 angular head housing [D]. Yanshan University, 2023.

[30] Ma Shuaiwei. Design and aerodynamic performance of window air curtain system for passenger cars based on CFD [D]. Chongqing Jiaotong University, 2023.